Journal of Marine Research, 65, 147–168, 2007

Dissipation in hydraulic transitions in flows through abyssal channels

by S. A. Thorpe[1,2]

ABSTRACT

There is growing evidence from observations that mixing occurs in hydraulic jumps, or flow transitions, downstream of sills within channels connecting deep ocean basins or within submarine canyons on the flanks of mid-ocean ridges. Models with continuous profiles of velocity and density upstream and downstream of a transition, but conforming to continuity conditions, are devised to represent the mixing that occurs in a hydraulic jump in a stratified shear flow of finite depth moving over a horizontal boundary in a deep fluid. These are used to assess the conditions in which transitions may occur and to provide an estimate of the loss in the flux of energy carried by the flow. An increase in the thickness of the stratified flow layer is necessary as water passes through a transition. The rate of loss of energy flux per unit channel width in a transition is typically of order $6\rho h(g\beta h)^{3/2}$, where h is a measure of the thickness of the flow before transition, g the acceleration due to gravity and $\beta = \Delta\rho/\rho$ ($<<1$), where $\Delta\rho$ is half the difference in density between that in the flow approaching the transition and that in the overlying fluid, and ρ is the mean density. The mean rate of loss of energy in a transition in the flow of Antarctic Bottom Water over just one of the 6–8 sills in the Romanche Fracture Zone is estimated to be of order 60 MW (6×10^7 W).

1. Introduction

There is presently circumstantial, but no definitive, evidence of the existence of hydraulic jumps in the abyssal ocean. A reduction in the density of Antarctic Bottom Water (AABW) flowing over sills or through constrictions in passages connecting neighboring ocean basins is evidence that mixing occurs. Bryden and Nurser (2003) argue that mixing in the Vema Channel and the Romanche Fracture Zone (RFZ) results in an eddy diffusivity that is an order of magnitude greater than Munk's (1966) estimate of a mean value of about 1×10^{-4} m^2 s^{-1} at depths exceeding 1500 m. They conjecture that the AABW flows 'over the sill in some kind of hydraulically controlled process and then there is "strait" mixing' (of unspecified nature) 'as the dense water plunges down into the next basin.' In the RFZ, the only deep ocean passage in which measurements of turbulence appear to have been made, Polzin *et al*. (1996) show that the rates of turbulent dissipation in the AABW reach values exceeding 1×10^{-6} W kg^{-1} and suggest the possibility of internal hydraulic jumps,

1. School of Ocean Sciences, University of Bangor, Menai Bridge, Anglesey, United Kingdom.
2. Corresponding address: 'Bodfryn', Glanrafon, Llangoed, Anglesey, LL58 8PH, United Kingdom. ***email: oss413@sos.bangor.ac.uk.***

but are unable to establish from their data that jumps occur. Ferron *et al*. (1998) estimate the rate of dissipation of turbulent kinetic energy in the flow of AABW through the Chain and Romanche Fracture Zones from CTD measurements of temperature fine structure, and find that the diapycnal flux there, whilst not exceeding that in the downstream Sierra Leone and Guinea Abyssal Plains, is a substantial fraction of the flux that occurs over the much greater area of these adjoining basins. They observe large density overturns downstream of sills in the RFZ, extending well above the bottom and indicative of intense mixing. They conjecture that dense fluid, initially forced by a zonal baroclinic pressure gradient, accelerates under gravity in spilling into valleys after passing over sills but, like Polzin *et al*., do not have data with the spatial resolution down the passage required to establish whether or not hydraulic jumps occur. In canyons flanking the mid-Atlantic Ridge, Thurnherr *et al*., (2005) find a strong association between along-canyon density gradients, evidence of mixing, and the presence of cross-canyon sills. Hydraulic jumps are identified as one of the main candidate processes that may account for the mixing, but no direct observations that establish their presence or absence are available.

Extensive reference to related studies of flow near and over topography is given by Baines (1995). It is customary in the study of internal hydraulic jumps to adopt a two-layer approximation to the flow both upstream and downstream of the transition, with the density being preserved in each layer (e.g., Holland *et al*., 2002). In reality, however, mixing takes place, and even if upstream of a hydraulic jump the flow may be represented as two-layer (which it rarely is), the density and velocity profiles cannot remain discretely layered downstream of a jump. Turbulent mixing modifies both profiles. In contrast to earlier models, we here devise models of a continuously stratified shear flow chosen to represent that passing through the RFZ. It is assumed that turbulent mixing occurs and reduces the density of the flow as it passes through a hydraulic jump.

Our objective is to examine the conditions necessary for hydraulic jumps to occur and to obtain estimates of the associated rate of loss of energy flux. The unconventional approach is to select plausible profiles of velocity and density before and following a transition, and to examine the constraints imposed on the flow upstream of a transition by the conditions that the fluxes of volume, mass and momentum are conserved, and that the flux of energy must not increase, through a turbulent transition. For physically plausible flows, it is found possible to determine the loss of energy flux and hence to estimate the rate of energy dissipation in possible transitions. We shall conclude that it is unlikely that the total dissipation occurring in hydraulic jumps in the flows in abyssal channels contributes significantly to the rate, about 2 TW, estimated by Munk and Wunsch (1998) to be needed to support mixing in the abyssal ocean.

2. The flow in the Romanche Fracture Zone

Of all the channels connecting the deep basins in the Atlantic through which the AABW spreads northwards or eastwards, that where most is known of the local dynamics is the RFZ. This has been studied by Polzin *et al*. (1996), Mercier and Morin (1997), Mercier and

Speer (1998) and Ferron *et al*. (1998), and we shall use values observed in this channel as a basis on which to select plausible velocity and density variations for the model studies of Sections 3–5. The channel is about 30 km wide, and Polzin *et al*. estimate the mean flux through it to be about 1 Sv (compared to earlier values ranging from 1.2 to 5.1 Sv). Mercier and Speer find speeds varying from about 0.2 to 0.3 m s^{-1} but at a location before the AABW passes over the main sill. The vertical change in potential density near the diffuse top of the AABW is typically about 0.03–0.05 kg m^{-3} in 500 m, but immediately downstream of sills changes of about 0.05 kg m^{-3} over 200 m are observed by Polzin *et al*. The density change over the thickness of the AABW is therefore $2\Delta\rho \approx 0.05$ kg m^{-3}.

There appear to be 6–8 sills that may affect the eastward flow through the Fracture Zone and, although comprehensive data are presently lacking, an overall increase in potential temperature of the AABW of about 0.2 °C, corresponding to a decrease in potential density of order 0.02 kg m^{-3}, is observed as the flow passes through a section with at least 3 sills (Ferron *et al*., 1998). Mercier and Morin (1997) observe a reduction in potential density of about 0.06 kg m^{-3} as the flow passes over 5 sills in a distance of about 220 km. Polzin *et al*. (1996) find an increase of potential temperature of about 0.5 °C over a distance of 80 km after passing the main, and subsequently 3 other sills, corresponding to a change in potential density of about 0.05 kg m^{-3}. Although the measurements of velocity are insufficient to determine whether some blocking of the flow near the bottom may occur upstream of sills—and hence whether density changes from one side of a sill to another are associated with blocking rather than with mixing—the section of potential temperature and corresponding velocity profiles measured by Polzin *et al*. (their Fig. 2) indicates that much of the density changes are in the lee of sills or constrictions in the channel, and are associated with intense mixing. We shall suppose that the majority of the density changes occur in transitions in the lee of sills, each leading to a mean decrease of about $(1 - \delta)\Delta\rho = 0.012$ kg m^{-3} in potential density, and so $\delta \approx 0.52$. We adopt $g\beta = g\Delta\rho/\rho = 2.5 \times 10^{-4}$ m s^{-2} and $\delta = 0.52$ in the later calculations.

The thickness of the AABW is roughly 500 m with flow accelerating and the thickness of the flow possibly being reduced as it passes over the sills. The maximum observed current observed by Polzin *et al*. is about 0.5 m s^{-1}, but their relatively coarse horizontal sampling may underestimate the flows just upstream of hydraulic jumps. Richardson numbers estimated over 100 m with a High Resolution Profiler (HRP) within the AABW downstream of the main sill are found that are less than about 0.25, suggesting that flows may possibly be unstable to Kelvin-Helmholtz instability. The largest observed vertical gradient in horizontal velocity is also just downstream of a sill (Sill 2 as identified by Polzin *et al*.) where the speed increases downwards from near zero to about 0.5 m s^{-1} over a vertical distance of 200 m, the flow being relatively uniform below the shear layer.[3]

3. Corresponding values of buoyancy frequency are $N = [g\Delta\rho/\rho d_1]^{1/2} \approx [10 \times (0.03–0.05)/(1000 \times 500)]^{1/2} = (0.77–1.0) \times 10^{-3}$ s^{-1}; if $Ri = ¼$, $dU/dz = 2N$, so over, say, (200–300) m, the velocity must change by $2 \times (200–300) \times (0.77–1.0) \times 10^{-3} = (0.31–0.6)$ m s^{-1}, consistent with the magnitude of the observed flows.

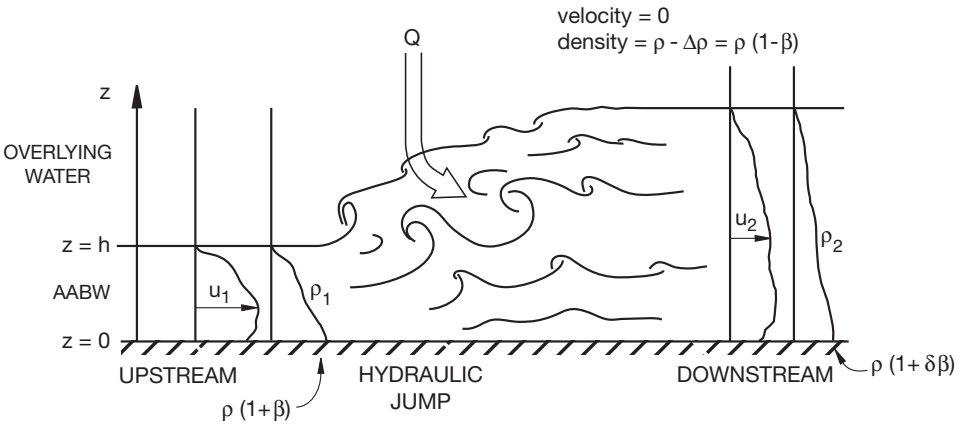

Figure 1. Sketch of a stationary hydraulic jump or transition between one steady stratified shear flow (of speed u_1, density ρ_1) and a second steady flow (of speed u_2, density ρ_2). Both flows are from left to right. Fluid is entrained at a rate, Q, from the upper layer, supposed for simplicity in the models to be at rest and of uniform density.

We shall consider models of a stationary transition in a steady flow over a horizontal plane at $z = 0$ as sketched in Figure 1. In reality, as in surface hydraulics, the location of transitions may be determined by where critical conditions are reached in a flow that is slowly accelerating in passing over and down the lee side of a sill, or within a narrowing channel. It is supposed here that flows are steady and that the bottom slope (generally less than about 5° in the RFZ), although possibly determining the location of transitions, plays no part in the dynamics or energy loss in the transitions themselves. There are no velocity and density profiles immediately upstream and downstream of possible jumps in the RFZ, but the measured profiles of potential density over the main sill by Mercier and Morin (1997) indicate, in increasing depth, weak gradients lying above an interfacial layer of steadily (and roughly linearly) increasing density beneath which there is a relatively small mixed bottom layer (e.g. Fig. 12, station 20 of Mercier and Morin's paper), whereas downstream of sills the interfacial layer is relatively thin (e.g., stations 63, 67). A similar evolution in density is suggested by the data of Polzin *et al*. (1996). There is even less information about the velocity profiles, but those that have been measured suggest strong shear layers corresponding to the interfacial density layers, with relatively low flow in the overlying water mass (e.g., Polzin *et al.,* 1996, Fig. 2b).

Two models of the flow are adopted, models A and B, the first perhaps more closely representing the flows that have been observed and the second the flow that might occur as water cascades in a density current or inclined plume in the lee of a sill. The effects of cross-channel variation and of rotation, negligible in the RFZ because it is near the Equator but perhaps important in other channels, are not included in the models.

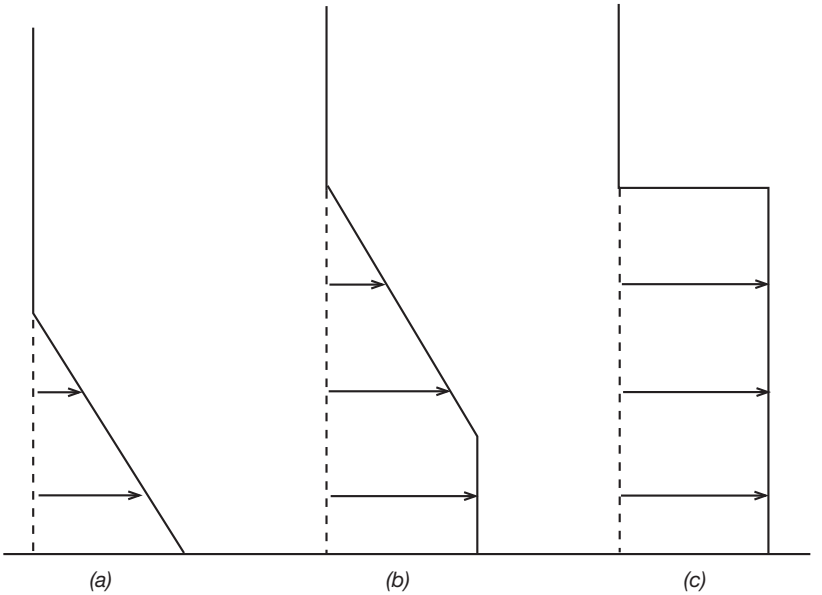

Figure 2. Profiles of the velocity profiles of model A when $r_i = d_i/h_i$ ($i = 1, 2$) equals (a) 1, (b) 0.5 and (c) 0. Density profiles selected in the model are of similar shape. The flow in (a) is stable for all values of the Richardson number, (b) is unstable when the Richardson number is less than ¼, whilst the two-layer flow (c) is always unstable for sufficiently short waves.

3. Model A

This model has discontinuous gradients of velocity, u, and density, ρ. In the flow upstream (subscript 1) of a transition in model A these are

$$u = U_1 \text{ and } \rho = \rho + \Delta\rho \text{ in } 0 < z < h_1 - d_1;$$

$$u = U_1(d_1 - z + h_1)/2d_1 \text{ and } \rho = \rho - (z - h_1)\Delta\rho/d_1 \text{ in } h_1 - d_1 < z < h_1 + d_1; \text{ and} \quad (1)$$

$$u = 0 \text{ and } \rho = \rho - \Delta\rho \text{ in } z > h_1 + d_1,$$

and those downstream (subscript 2) are

$$u = U_2 \text{ and } \rho = \rho + \delta\Delta\rho \text{ in } 0 < z < h_2 - d_2;$$

$$u = U_2(d_2 - z + h_2)/2d_2 \text{ and } \rho = \rho + \Delta\rho[h_2(\delta + 1) + d_2(\delta - 1) - (\delta + 1)z]/2d_2$$
$$\text{in } h_2 - d_2 < z < h_2 + d_2;$$

and

$$u = 0 \text{ and } \rho = \rho - \Delta\rho \text{ in } z > h_2 + d_2, \quad (2)$$

representing a stratified dense fluid flowing over a level bottom and below a static deep layer. The velocity and density are uniform above the plane boundary to levels $z = h_i - d_i$ ($i = 1, 2$). The density in the lower layer downstream of the transition has, however, been reduced by processes of mixing in the transition by a factor, δ, from $\rho + \Delta\rho$ to $\rho + \delta\Delta\rho$, a fractional change in density of $(1 - \delta)\Delta\rho$. The factor δ is less than or equal to unity because the maximum density in the flow, $\rho + \Delta\rho$, upstream of the transition cannot be increased through mixing as it passes through the transition. Above the levels $z = h_i - d_i$ ($i = 1, 2$), there are regions of thickness $2d_i$ in which the velocity and density decrease continuously and linearly to uniform values $u = 0$ and $\rho = \rho - \Delta\rho$ in the overlying ocean. Being of uniform density, the stationary upper layer cannot transfer energy upwards from the transition by radiating internal waves, a process of energy loss from transitions that may occur in the real stratified ocean but which, for simplicity, is disregarded here. Profiles of velocity with $r_i = d_i/h_i$ ($i = 1, 2$) equal to 1, 0.5 and 0 are shown in Figure 2. The density profiles are of similar shape.

One objective is to discover the upstream conditions necessary for the occurrence of a stationary transition. Three conservation conditions are adopted, those of volume flux, mass flux and momentum flux. We seek jumps of large amplitude with substantial loss in energy flux and relatively negligible loss in momentum flux. It is assumed that there is a flux, Q, of fluid of density $\rho = \rho - \Delta\rho$ entrained into the flow from the upper stationary layer. Conservation of volume flux ($\int udz$) gives

$$U_1 h_1 + Q = U_2 h_2 \tag{3}$$

and, using (3), conservation of mass flux ($\int \rho udz$) gives

$$U_1(h_1 - 2d_1/3) - Q = U_2(\delta h_2 - \delta d_2/3 - d_2/3). \tag{4}$$

Writing $r_i = d_i/h_i$ with $0 \leq r_i \leq 1$ (values taken ≤ 1 since values exceeding 1 lead to profiles of velocity and density that are identical to those with $r_i = 1$), and $q = h_2/h_1$, Eqs. (3) and (4) give

$$U_2 = 2U_1(3 - r_1)/[q(1 + \delta)(3 - r_2)]. \tag{5}$$

The fractional change in density of the flow through the transition is $(1 - \delta)\Delta\rho/\rho$ or $(1 - \delta)\beta$ where $\beta = \Delta\rho/\rho$. We shall suppose $\beta << 1$.

From Eqs. (3) and (5), the ratio of the entrainment flux to the flux of the flow upstream of the jump is

$$Q/U_1 h_1 = 2(3 - r_1)/[(1 + \delta)(3 - r_2)] - 1, \tag{6}$$

and since this must be ≥ 0 if there is entrainment, $(1 + \delta) \leq 2(3 - r_1)/(3 - r_2)$ or

$$\delta \leq (3 - 2r_1 + r_2)/(3 - r_2), \tag{7}$$

imposing a bound on the value of δ for given r_1 and r_2 (or a bound on the width of the downstream interface, r_2, for given upstream interface thickness, r_1, and mixing represented by δ).

Conservation of the flux of momentum ($\int(\rho u)u dz + \int p dz$, where p is the pressure), assuming that the entrained flux, Q, carries no momentum, and use of Eq. (5) leads to

$$U_1^2/g\beta h_1 = q[q^2(1+\delta)(3+r_2^2) - 2(3+r_1^2)]/ \{2(3-r_1)\{(q - [4/(1+\delta)^2][(3-r_1)/(3-r_2)]\}. \quad (8)$$

Eq. (8) is an expression that determines the speed, U_1, of a flow with the given upstream velocity and density structure that can undergo transition to the specified downstream flow state. Singularities in U_1 are found where $q = q_1 \equiv [4/(1+\delta)^2][(3-r_1)/(3-r_2)]\}$, where $U_1^2/g\beta h_1$ tends to infinity, and at $q = q_2 \equiv \{2(3+r_1^2)/[(1+\delta)(3+r_2^2)]\}^{1/2}$, where $U_1^2/g\beta h_1$ tends to zero.

The Richardson numbers in the layer $h_i - d_i < z < h_i + d_i$ ($i = 1, 2$, respectively) in the flows upstream and downstream of the transition are

$$Ri_1 = 4g\beta d_1/U_1^2 \quad (9)$$

and

$$Ri_2 = 2g\beta d_2(1+\delta)/U_2^2, \quad (10)$$

respectively, and these can be expressed in terms of q, r_1 and r_2 using Eqs. (5) and (8). The flows with the chosen density and velocity profiles are found to be unstable to small disturbances when $Ri_i < ¼$ except when $r_i = 1$ ($i = 1, 2$) when they are stable at all $Ri_i \geq 0$. When $r_i = 0$, as shown in Figure 2c, the profiles reduce to two layers, known to be unstable to sufficiently short wavelength disturbances. For a transition to a stable flow, $r_2 = 1$ or $Ri_2 > ¼$.

If there is no internal source of energy the flux of energy in the flow ($\int(\rho u^2/2)u dz + \int p u dz + \int g\rho z dz$) must be conserved or decrease as it passes through the transition. Although in reality the flow upstream of a transition may be turbulent, it is assumed in both models, A and B, that the fluxes of turbulent energy upstream and sufficiently far downstream of the transition are negligible or approximately equal so that neither appear in the equation of conservation of energy flux. It is also assumed that the flux of kinetic energy of the entrained flow is much less than the rate of loss of energy flux estimated disregarding the kinetic energy of the entrained fluid, an assumption to which we return in Section 6. After some algebra, and use of Eqs. (4) and (5) and the condition $\beta << 1$, the rate of loss of energy flux, ΔE, per unit channel width can be written in nondimensional form, E, as

$$E = \Delta E/[\rho h_1(g\beta h_1)^{3/2}] = (U_1^2/g\beta h_1)^{3/2} \{2 - r_1 - 8(2-r_2)(3-r_1)^3/[(1+\delta)^3(3-r_2)^3 q^2]\}/4 + (U_1^2/g\beta h_1)^{1/2}[2 - 2r_1/3 + r_1^2/3 - q(3-r_1)(1 - r_2/3 + r_2^2/6)/(3-r_2)], \quad (11)$$

where $U_1^2/g\beta h_1$ is given by Eq. (8). Without a source of energy, E cannot be negative in a physically realisable flow.

A final condition is applied, that no further transition of the flow downstream of a transition is possible without change to the velocity and density profiles. The selected downstream profiles resulting from a possible transition are then, in this sense, stable to further transitions. A second transition, if possible, would be to a flow with no further change in density of the lower layer and with an interface thickness characterised by $r_3 = r_2$. Applying Eq. (6) with $\delta = 1$ implies that there will be no entrainment from the upper layer in such a transition, and writing Eq. (8) for a transition from the present downstream state (suffix 2) to a further downstream state (suffix 3) (with $\delta = 1$ and writing $r_3 = r_2$) we derive the condition for a second transition to occur:

$$U_2^2/g\beta_2 h_2 = q_2(q_2 + 1)(3 + r_2^2)/(3 - r_2), \tag{12}$$

where $q_2 = h_3/h_2$ and $\beta_2 = (1 + \delta)\beta_1/2$. This may be written

$$U_2^2/g\beta_2 h_2 \geq (3 + r_2^2)/(3 - r_2) \tag{13}$$

since $q_2 \geq 1$ (which must be so for a loss of energy flux in this second transition). Use of Eq. (5) then implies that, for a second transition to occur,

$$4(U_1^2/g\beta_1 h_1)(3 - r_1^2)/[q^3(1 + \delta)3(3 + r_2^2)/(3 - r_2)] \geq 1. \tag{14}$$

The implications of these relations for $U_1^2/g\beta_1 h_1$, E and stability, with parameters representing the flow in the RFZ, are considered in Section 5.

4. Model B

The velocity and density profiles may, in general, be taken as $u_i = U_i F(z/h)$ and $\rho_i = \rho[1 - \beta + 2\beta f_i(z/h)]$ in $0 \leq z \leq h$, with $i = 1$ upstream and $i = 2$ downstream of the transition. As in model A, the velocity is chosen to be zero and the density is constant, $\rho[1 - \beta]$, above the flow domain, $z \leq h$. Equations expressing flux conservation are given in Appendix A. An entrainment factor, P, is defined in Eq. (A6) in terms of the ratio of the flux of water entrained from the upper stationary layer to the flux before a transition.

Profiles of velocity and density upstream of a transition are chosen in model B to represent water cascading down a gentle slope. The classical laboratory mean velocity and density profiles of Ellison and Turner (1959; see also Turner, 1973, Section 6.2.4) and data from recent studies of cascading water in Lake Geneva (Fer *et al*., 2002) are represented by choosing a velocity jet and exponential density,

$$\begin{aligned} F_1 &= [\pi(1 - z/h)]^4 \sin[\pi(1 - z/h)] \text{ and} \\ f_1 &= [\exp(-\alpha z) - \exp(-\alpha h)]/[1 - \exp(-\alpha h)], \end{aligned} \tag{15}$$

upstream of the transition as shown in Figure 3. The selected form of F_1 has a maximum, 23.61, at a level $z/h = 0.182$ close to that of the observations, and is zero at $z = 0$ and h. A

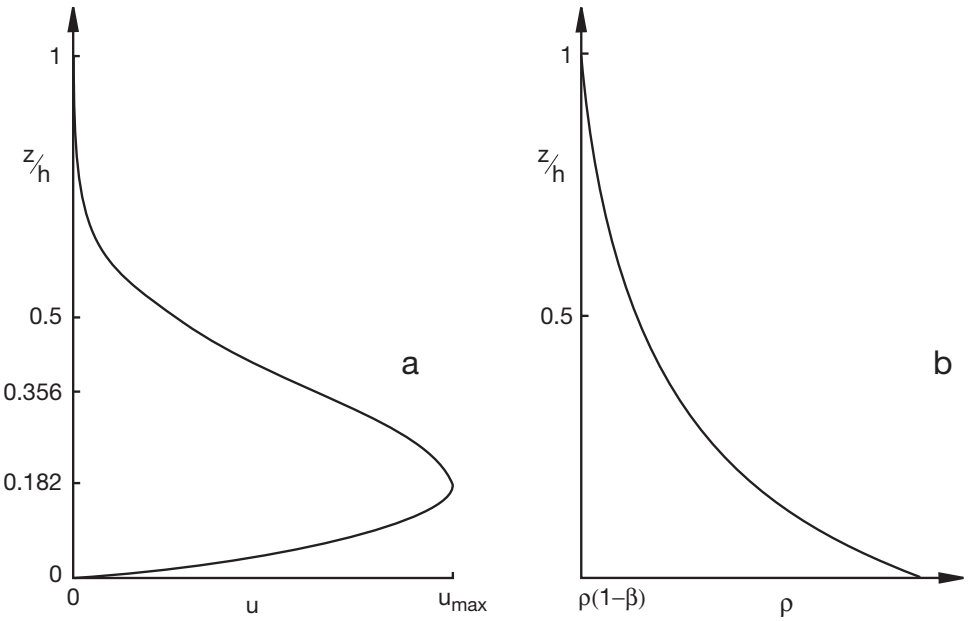

Figure 3. (a) Velocity and (b) density profiles of model B representing an inclined plume.

choice of $\alpha h = 3.5$ is found to give a reasonable fit to observed density profiles and is used in the examples below.

The Richardson numbers of the mean flow in inclined turbulent plumes, density currents flowing down slopes, vary with height above the boundary and the minimum value is less than the Miles-Howard critical value of 0.25. Turner (1973) suggests that a value of about 0.1 in the near-uniform velocity gradient above the flow maximum is a marginal value. (Values of about 0.1 are indeed observed in Lake Geneva.) We characterize the Richardson number of the profiles, Eq. (15), by its value, Ri_{inf1}, at the inflexion point at $z/h = 0.356$ in the velocity profile upstream of a transition. When $\alpha h = 3.5$, $Ri_{inf1} = 0.2326 g\beta h/u_{max}{}^2$, where $u_{max} = 23.61 U_1$ is the maximum speed of the flow upstream of the transition.

Three forms of the velocity and density profiles downstream of a transition are considered, spanning the possible likely shapes: profiles that are unchanged from those upstream (i.e., as in Eq. (15)), a profile of velocity identical to that upstream but a linear density profile, $f_2 = \delta_1(1 - z/h)$), representing partial but incomplete mixing, and velocity and density profiles in which mixing completely homogenizes the fluid so that both velocity and density that are uniform, $F_2 = 1$ and $f_2 = \delta_1$ at height $z < h_2$. The rate of loss of energy flux, ΔE, in a possible transition found using Eq. (A12) is written in nondimensional form, $E = \Delta E/[\rho h_1 (g\beta h_1)^{3/2}]$, as in Eq. (11).

We apply the results to the RFZ in Section 5.

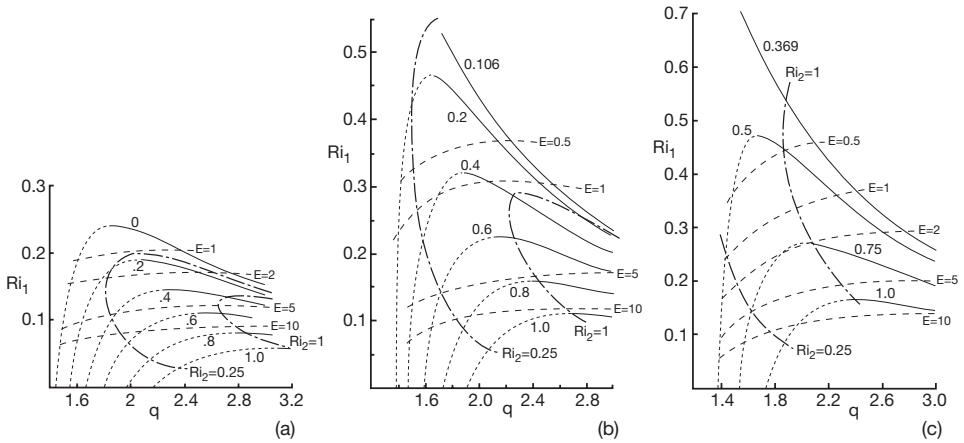

Figure 4. Transitions in a flow of model A, when r_1 = (a) 0.5, (b) 0.8, and (c) 1.0, and $\delta = 0.52$, corresponding to the RFZ value. Values of the jump amplitude, q, and upstream Richardson number, Ri_1, at which transitions are possible are shown for a variety of labelled values of r_2. Stable transitions (those when second transitions, preserving the shape of the density and velocity profiles, cannot occur without further entrainment) are shown by continuous lines for given values of r_2. Unstable transitions are indicated by dotted lines. The dashed lines are curves of constant nondimensional loss in energy flux, E, and the dot-dash curves are those of constant Ri_2, the Richardson number in the flow downstream of a transition.

5. Estimates of the rate of loss of energy flux in the RFZ

Figure 4 shows the conditions in which transitions are possible using model A with $\delta = 0.52$ as the Richardson number, Ri_1, and the jump amplitude, q, are varied. The full curves give values of q and Ri_1 at which solutions to Eq. (8) are found and transitions are possible. Their dotted extensions are unstable transitions where Eq. (14) is satisfied and for which a further transition can occur with no further entrainment. The dashed curves show values of the nondimensional energy flux, E, given by Eq. (11), and the dot-dashed curves are where $Ri_2 = 0.25$, the limit for Kelvin-Helmholtz instability, and 1.

Three cases, r_1 = (a) 0.5, (b) 0.8, and (c) 1.0, are taken for illustration. Each shows values of Ri_1 derived using Eqs. (8) and (9) over a range of values, r_2. In (a), the largest possible value of Ri_1 for which a transition can occur is 0.242 when $r_2 = 0$. (In this case the flow downstream of the transition has a Richardson number less than 0.25 and, as mentioned earlier, is therefore unstable.) In Figure 4b, $r_1 = 0.8$ and r_2 is constrained by Eq. (7) to lie between 0.106 and 1.0; since $\delta = 0.52$, $1 \geq r_2 \geq 1.312r_1 - 0.947 = 0.106$, this value corresponding to zero entrainment. Similar curves for $r_1 = 1.0$ are shown in Figure 4c. In this case $1.0 \geq r_2 \geq 0.369$ and Ri_1 must be less than 0.64 for a transition to occur.

Figure 5 illustrates the sensitivity of the results to δ, by changing δ from its value of 0.52 in the RFZ to (a) 0.1 and (b) 0.7 when $r_1 = 0.8$. These may be compared to Figure 4b at the same value of r_1.

Several conclusions can be drawn from the two figures. Stable transitions occur only

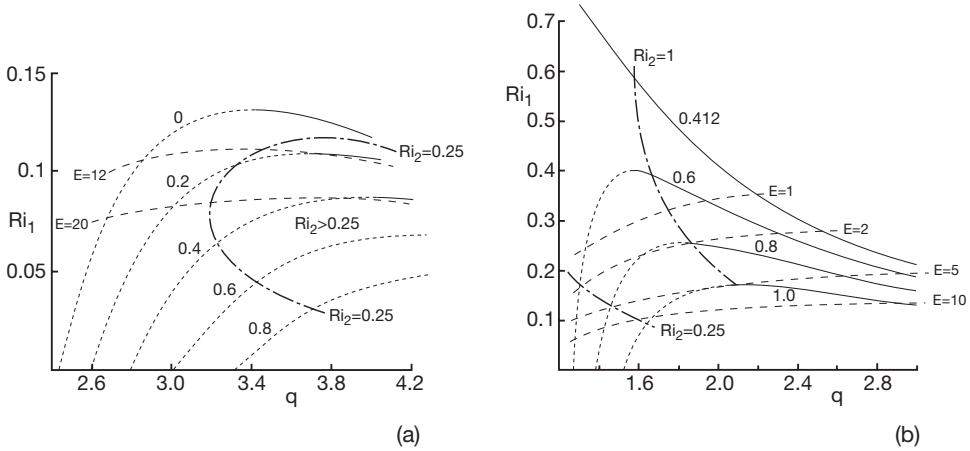

Figure 5. Transitions in a flow of model A, when $r_1 = 0.8$ and δ = (a) 0.1 and (b) 0.7, spanning across the value, $\delta = 0.52$, in the RFZ. The curves at specified values of r_2, E and Ri_2, are drawn as in Fig.4.

when $q > 1$, that is when the thickness of the flowing stratified layer increases. Transitions are possible only if Ri_1 is sufficiently small, e.g., less than 0.53 if $\delta = 0.52$ and $r_1 = 0.8$ (Fig. 4b). The maximum value of Ri_1 for any transition between the selected upstream and downstream density and velocity profiles to be possible with $\delta = 0.52$ is 0.718, when $r_1 = 1$ and $r_2 = 0.369$. The upper limit of Ri_1 decreases as r_2 increases for given r_1 and δ. The greatest value of Ri_1 for which transitions can occur for given r_1 and r_2 decreases as δ decreases. The transitions with q less than its value at which Ri_1 is greatest for given r_1 and r_2 are all unstable to further possible transitions; there is only one possible stable transition for given r_1 and r_2. Generally transitions of greater amplitude, q, but the same r_2 require smaller upstream Richardson numbers, Ri_1. Smaller values are also required to produce transitions as the relative thickness of the interfaces, r_2, increases at a given amplitude, q. For a fixed δ, the nondimensional loss in energy flux, E, increases slowly for given the upstream Richardson numbers, Ri_1, and fixed r_1 as the jump amplitude, q, increases (r_2 decreasing at fixed r_1), although values of E at given Ri_1 and q decrease as r_1 decreases at fixed δ. It is notable, however, that the loss in energy flux, E, is relatively insensitive to changes in r_2 and q, and even to r_1 and δ, being of order 2 when the upstream Richardson numbers, Ri_1, are near the limit, 0.25, at which the flow is unstable to Kelvin-Helmholtz instability. Values of order 10 are found when Ri_1 is of order 0.1, a subcritical Richardson number that might be attained in a flow that has accelerated in passing over a sill.

Model B with density coefficient $\alpha h = 3.5$ has been used to find values of q, Ri_{infl} and E corresponding to possible transitions. When the velocity and density profiles have the same shape before and after transition, the entrainment factor, P, given by Eq. (A8), is equal to $2/(1 + \delta)$. Examples with $\delta = 0.1$, 0.52 (corresponding to the RFZ), and 0.7 ($P = 1.82$, 1.32 and 1.18, respectively) are shown in Figure 6a–c, for ranges of q including the

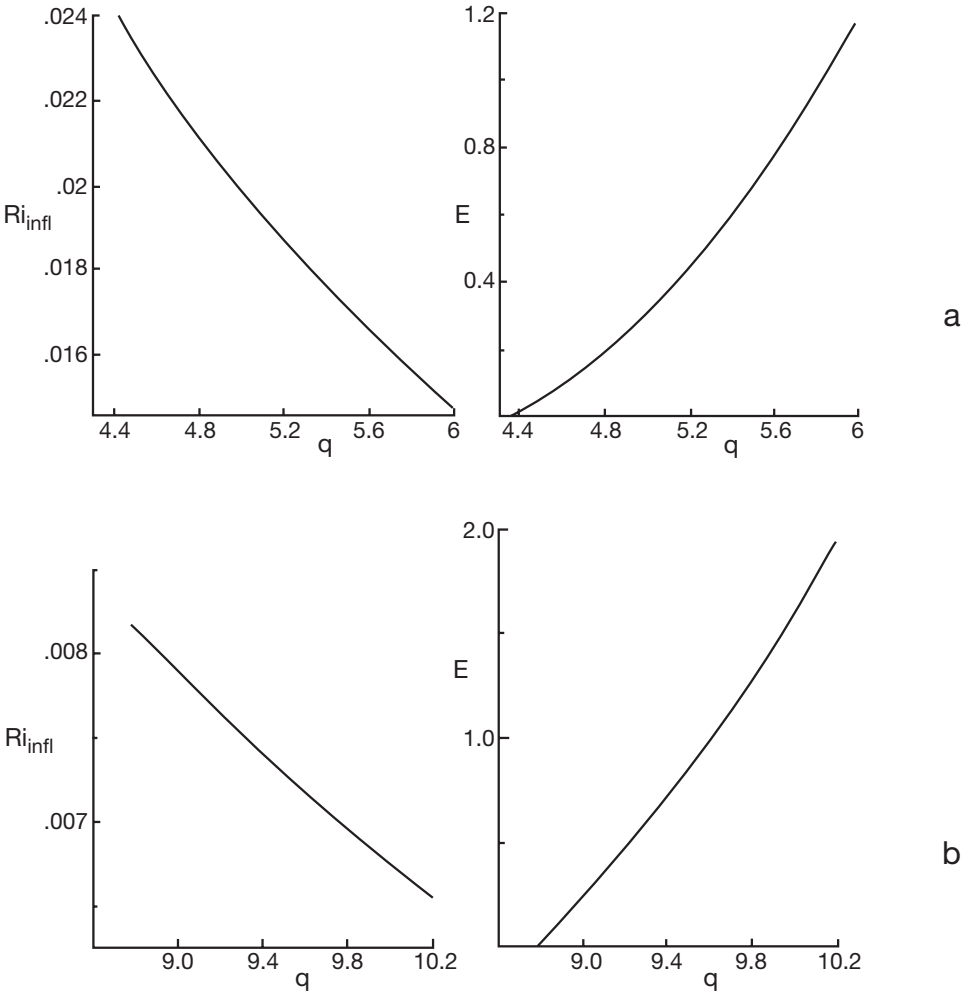

Figure 6. Transitions in a flow of model B with density coefficient $\alpha h = 3.5$. The curves show (left) the values of jump amplitude, q, and upstream Richardson number, Ri_{infl}, at the inflexion point for which transitions are possible and (right) the corresponding values of the nondimensional rate of loss in energy flux, E. Solutions are shown when the velocity and density profiles have the same shape before and after transition with $\delta =$ (a) 0.1, (b) 0.52 (corresponding to the RFZ), and (c) 0.7. Part (d) shows values when $\delta = 0.1$ for possible transitions when the exponential density profile upstream is changed by mixing to a linear profile downstream.

smallest values for which the nondimensional loss in energy flux, $E > 0$. The transitions are stable to further transitions within the range of q shown and at higher q: Eq. (A13) cannot be satisfied. As in model A, the Richardson number at the inflexion point, Ri_{infl}, must be sufficiently small (or ${u_{max}}^2/g\beta h$ sufficiently large) for a transition to be possible. The Richardson number at the inflexion point, Ri_{infl}, required for a transition to occur

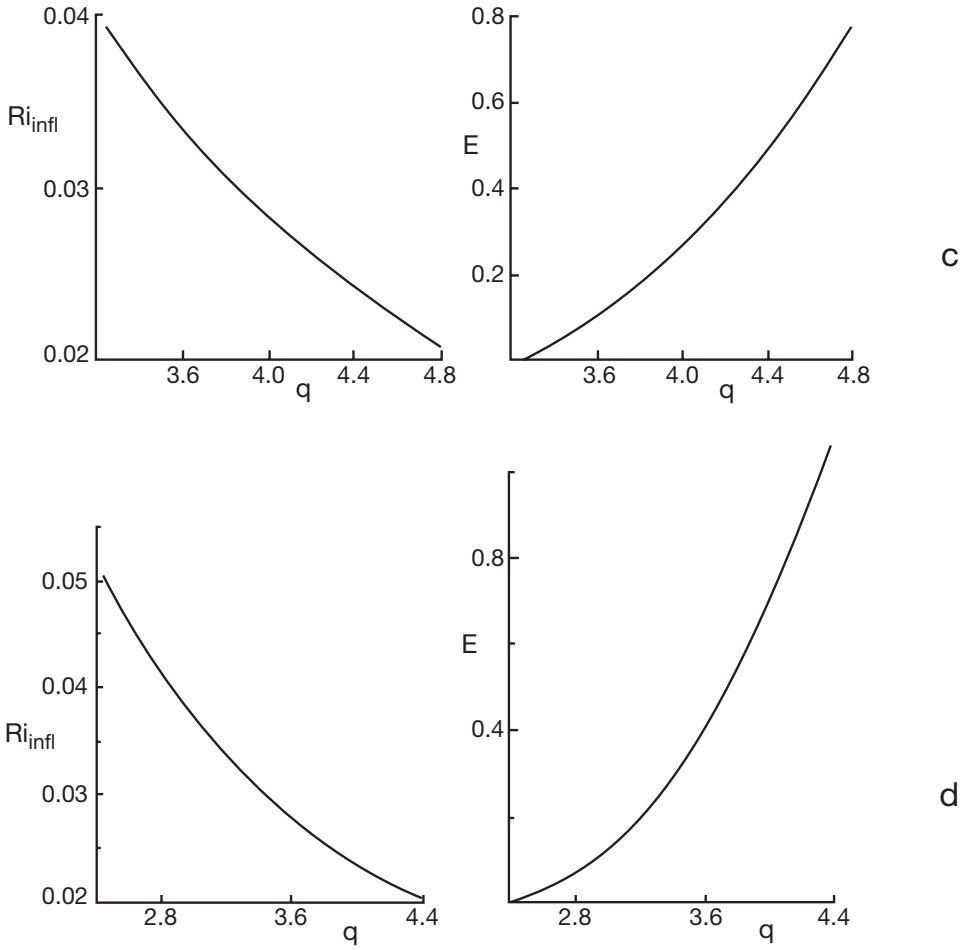

Figure 6. (Continued)

decreases as the amplitude, q, of transitions increases. For example when $\delta = 0.52$ as in the RFZ, solutions with $E > 0$ are found only if $u_{max}^2/g\beta h > 11.79$ and $q > 4.57$.[4] The minimum Ri_{infl} needed for transition to occur increases as δ increases and the minimum possible jump amplitude decreases; the greater mixing implied by smaller δ requires larger jumps and lower Ri_{infl} or greater $u_{max}^2/g\beta h$. Values of E are of order unity for moderate values of Ri_{infl} and q.

When the density profile downstream of a transition is linear, transitions can only be found with $P = 1.18/(1+\delta)$ or, since $P \geq 1$, when $\delta \leq 0.18$. No transition is therefore

4. Values of $u_{max}^2/g\beta h$ estimated in inclined plumes over uniform slopes are typically 2–4, suggesting their stability to the transitions considered here.

Table 1. Estimates of maximum velocity, U_1, and rate of loss of energy flux in the RFZ, $l\Delta E$, derived using model A for various representative values of r_1, r_2, and shear layer thickness, $h_1 + d_1 = h_1(1 + r_1)$. The width of the channel, l, is taken as 30 km, $\delta = 0.52$ and $g\beta = 2.5 \times 10^{-4}$ m s^{-2}. Values of U_1 are related to Ri_1 by Eq. (9) and Ri_2 is found using Eq. (10). R is equal to the rate of loss of energy flux divided by the flux of kinetic energy upstream of the transition. The entrainment ratio given by Eq. (6), Q/U_1h_1, is the ratio of the entrained flux to the flux of water in the flow approaching a possible transition.

r_2	$U_1^2/g\beta h_1$	Ri_1	Ri_2	q	h_1 (m)	$h_1 + d_1$ (m)	$l\Delta E$ (MW)	U_1 (m s^{-1})	R	Q/U_1h_1
$r_1 = 0.5$										
0.2	11.30	0.177	0.54	2.4	100	150	21.07	0.532	0.125	0.175
0.2	11.30	0.177	0.54	2.4	150	225	58.06	0.651	0.125	0.175
0.2	11.30	0.177	0.54	2.4	200	300	119.18	0.752	0.125	0.175
0.2	11.30	0.177	0.54	2.4	250	375	208.19	0.841	0.125	0.175
0.4	13.82	0.145	0.76	2.4	100	150	38.14	0.588	0.167	0.126
0.4	13.82	0.145	0.76	2.4	150	225	105.11	0.720	0.167	0.126
0.4	13.82	0.145	0.76	2.4	200	300	215.76	0.831	0.167	0.126
$r_1 = 0.8$										
0.2	7.96	0.402	0.57	2.0	100	180	4.16	0.446	0.052	0.034
0.2	7.96	0.402	0.57	2.0	150	270	11.46	0.546	0.052	0.034
0.2	7.96	0.402	0.57	2.0	200	360	23.53	0.631	0.052	0.034
0.2	7.96	0.402	0.57	2.0	250	450	41.11	0.705	0.052	0.034
0.4	11.89	0.269	1.14	2.4	100	180	19.61	0.545	0.134	0.113
0.4	11.89	0.269	1.14	2.4	200	360	110.95	0.771	0.134	0.113
0.6	14.85	0.215	1.17	2.4	100	180	35.11	0.609	0.172	0.206
0.6	11.89	0.215	1.17	2.4	150	270	96.75	0.746	0.172	0.206
0.8	20.06	0.160	0.97	2.4	100	180	68.27	0.708	0.214	0.316
$r_1 = 1.0$										
0.4	8.39	0.477	1.13	2.0	100	200	5.00	0.458	0.069	0.012
0.4	8.39	0.477	1.13	2.0	200	400	28.27	0.648	0.069	0.012
0.4	8.39	0.477	1.13	2.0	250	500	49.39	0.724	0.069	0.012
0.6	11.15	0.359	1.09	2.0	100	200	11.94	0.528	0.108	0.097
0.6	11.15	0.359	1.09	2.0	200	400	67.56	0.747	0.108	0.097
0.8	17.34	0.231	1.36	2.4	100	200	39.00	0.658	0.182	0.196

possible if δ has the RFZ value, 0.52, but an example with $\delta = 0.1$ ($P = 1.07$) is shown in Figure 6d. Comparison with Figure 6b ($P = 1.32$) shows that smaller jump amplitudes, q, and greater minimum Ri_{inf1} are needed to support the reduced entrainment. Transitions to a mixed downstream state require $P = 0.875/(1+\delta)$ and are therefore impossible if $\delta > 0$; a transition leading from the assumed upstream profiles of velocity and density to uniform velocity and density profiles downstream is impossible for RFZ values.

Figures 4 (model A) and 6b (model B) with $\delta = 0.52$ correspond most closely to conditions in the RFZ. Tables 1 and 2 give some dimensional estimates based on the two models in conditions when transitions are stable. The values of model parameters such as q, r_1 and r_2 are selected to give a range of the maximum velocity of the flow approaching a

Table 2. Estimates of maximum velocity, u_{max}, and rate of loss of energy flux, $l\Delta E$, in the RFZ derived using model B. The width of the channel, l, is taken as 30 km, $\delta = 0.52$ and $g\beta = 2.5 \times 10^{-4}$ m s^{-2}. In this case the entrained flux is a fraction equal to 0.316 of the flux in the flow approaching a possible transition.

q	$u_{max}^2/g\beta h$	Ri_{inf1}	Ri_{inf2}	h (m)	u_{max} (m s^{-1})	$l\Delta E$ (MW)	R
4.5	10.00	0.0233	0.932	100	0.500	0.72	0.0172
4.5	10.00	0.0233	0.932	150	0.612	1.97	0.0172
4.5	10.00	0.0233	0.932	200	0.705	4.05	0.0172
5.0	11.77	0.0198	1.086	100	0.542	3.76	0.0704
5.0	11.77	0.0198	1.086	200	0.767	21.26	0.0704
5.5	13.71	0.0170	1.240	100	0.586	8.06	0.1202
5.5	13.71	0.0170	1.240	200	0.828	45.62	0.1202
6.0	15.83	0.0160	1.516	100	0.629	10.16	0.1662
6.0	15.83	0.0160	1.516	200	0.890	78.28	0.1662

transition (U_1 in model A and u_{max} in mode B) covering the levels likely within the RFZ. The most important numbers in the tables are the rates of loss of energy flux possible in transitions, $l\Delta E$, where $l = 30$ km is the width of the channel. These are generally less than 60 MW, higher values being found only in flows exceeding 0.7 m s^{-1}, greater than those presently reported.

In model A the Richardson numbers, Ri_1, have generally to be near the critical value of 0.25 for a transition to be possible and in all cases are less than 0.718. Transitions when $Ri_1 < 0.25$ may be a result of Kelvin-Helmholtz instability rather than hydraulics. The values of Ri_1 in model B are less than 0.25 in accord with the earlier remarks about the low Richardson numbers that occur in inclined plumes, but the downstream values Ri_1 are noticeably greater than 0.25, suggesting that a transition occurring in a cascading flow may result in a flow that is both statically and dynamically stable to small disturbances. The amplitude, q, of jumps in model B are much larger than those necessary for a stable, energy-flux-reducing transition of model A.

The tables also show that the ratio, R, of the rate of loss of energy flux divided by the incoming flux of kinetic energy ($l\int\rho u^3 dz/2$), is generally much less than unity. So is Q/U_1h_1, the ratio of the flux entrained from the overlying water to that of the water upstream of a transition shown in Table 1.

6. Discussion

Both models show that stable, energy-losing transitions involve an increase in the thickness of the flow; $q > 1$. Estimates are made of the rate of loss of energy flux in possible hydraulic jumps or transitions in the flow of water passing through the RFZ. An important assumption is that the flux of kinetic energy supplied by water entrained into the flow is small. This assumption is considered in Appendix B. The neglected flux may

enhance the loss of energy flux in possible transitions by about 30% at most, but the increase is generally much less.

Although more observations are required to constrain the models, we conclude that the present data are consistent with a rate of loss of energy in each of the several possible hydraulic transitions in the RFZ of about 40 ± 20 MW. The rate of dissipation of turbulent kinetic energy per unit mass, ε, observed by Polzin *et al.* is of order 10^{-6} W kg^{-1} downstream of the sills, so the mass of water within which dissipation occurs is of order $(4 \pm 2) \times 10^7$ W/10^{-6} W kg^{-1} = $(4 \pm 2) \times 10^{13}$ kg, or a volume of about $(4 \pm 2) \times 10^{10}$ m^3, provided turbulent dissipation is the only process though which the energy is lost in the hydraulic jumps. If the depth of the AABW is 300–500 m and the channel width is 30 km, the distance downstream of a jump affected by these high turbulence levels is relatively small, of order 1.3–5.0 km, respectively, or 10 times this distance if the mean dissipation rate is only 10^{-7} W kg^{-1}.

The estimated value of the loss of energy flux to mixing over a single sill in the Romanche Fracture Zone is greater than the value estimated in the whole Romanche Fracture Zone by Wunsch and Ferrari (2004). They use Ferron *et al's* estimate, $K_T = 1.5 \times 10^{-2}$ m^2 s^{-1} over the horizontal area, 10^3 km^2 of the Romanche Fracture Zone and determine the dissipation rate of turbulent kinetic energy per unit mass, ε, using $\varepsilon = 5N^2K_\rho$, with $K_\rho = K_T$. Assuming a depth of the flow of AABW of 500 m and a value, $N = 3.5 \times 10^{-4}$ s^{-1}, Wunsch and Ferrari find a mean value of $\varepsilon = 9 \times 10^{-9}$ W kg^{-1}, and integrate this to derive a total dissipation, $\int\int\int \rho\varepsilon dV$, of 4.5 MW, a factor of about 6 less than the lower of the values determined from Table 1 if there are 6 sills in the Zone and a factor of 80 less if an upper value of 60 MW at a single sill is accepted.

The discrepancy is not surprising, and is probably simply an indication of the uncertainty in both observations and model estimates. Observations by Wesson and Gregg (1994) near the Carmarinal Sill in the Straits of Gibraltar, where the mean dissipation is about 0.34 GW, demonstrate how relatively small are the areas within which the greatest dissipation occurs, and it is possible that within the RFZ (as is likely in other areas) the most extreme turbulence and greatest values of dissipation, are presently highly undersampled. If the mixing is dominated by the internal hydraulic jumps proposed here, it will certainly be localized. The photograph of the hydraulic jump in the lee of the Sierra Nevada range shown by Turner (1973; his Figure 3.11) illustrates just how large and abrupt transitions may be. The model estimates of dissipation may be too high if substantial energy is radiated by internal waves, excluded in the models.

Figures 4–6 show that the nondimensional loss in energy flux, E, is not very sensitive to changes in model, q or δ; the constant E curves in Figures 4 and 5, for example, are nearly horizontal and at comparable values of Ri_1. Values of $E = O(5)$ are found at values of Richardson number typically required for transitions. Including some small contribution from the flux of kinetic energy from the entrained flow, we might expect therefore that a value of $\Delta E = O[6\rho h_1 (g\beta h_1)^{3/2}]$ is typical of transitions, and that the results from the RFZ may be extended to other passages. A loss of 60 MW of energy flux, near the upper limit in

the RFZ, in each of 10^4 transitions would be sufficient to contribute only about 30% of the turbulent dissipation of about 2 TW found by Munk and Wunsch (1998) to be needed to sustain mixing in the deep ocean. Although Thurnherr *et al*. (2005) estimate that there may be $O(10^4)$ sills in the floors of canyons in mid-ocean ridges, it is unlikely that the dissipation near canyon sills can be as large as in the FRZ because of the relatively low (typically 0.02 m s^{-1}) flows and consequently smaller values of β required to maintain flows near marginal dynamic stability in the canyons. Even though the estimates of dissipation made here ignore mixing at the sides of the deep ocean passages, the value of 0.2 TW tentatively ascribed by Wunsch and Ferrari (2004) to mixing near the ocean floor as a result of the general circulation and the mesoscale eddy field (0.1 TW each) appears a plausible, if high, upper bound.[5] Further investigation is required, however, particularly to establish the existence and nature of hydraulic jumps in the abyssal ocean, and to discover whether they are augmented by transient flows driven by mesoscale eddies passing over the mid-ocean ridges, passages and canyons, or may contribute to more substantial rates of dissipation than estimated here.

APPENDIX A

Conservation equations in general form

We suppose that the steady flows upstream ($i = 1$) and downstream ($i = 2$) of a transition are given by

$$U(z) = U_i F_i(z/h_i) \text{ when } 0 \le z \le h_i, \tag{A1}$$

with the no-slip condition, $F_i(0) = 0$, and $F_i(1) = 0$, and that $U_i = 0$ when $z > h_i$. The corresponding density profiles are

$$\rho_i = \rho[1 - \beta + 2\beta f_i(z/h_i)] \text{ when } 0 \le z \le h_i, \tag{A2}$$

with $\rho_i = \rho(1 - \beta)$ when $z > h_i$, $df_i(z/h_i)/dz < 0$ to ensure static stability, and $f_1(0) = 1$, so defining $2\rho_0\beta$ as the density change from $z = 0$ to h_1. Conservation of volume flux through the assumed transition is satisfied by

$$U_1 h_1 \int_0^1 F_1(x)dx + Q = U_2 h_2 \int_0^1 F_2(x)dx, \tag{A3}$$

i.e.,

$$Q/U_1 h_1 \int_0^1 F_1(x)dx + 1 = U_2 h_2 \int_0^1 F_2(x)dx \Big/ \left(U_1 h_1 \int_0^1 F_1(x)dx \right), \tag{A4}$$

5. For comparison, Gregg *et al*. (2005) extrapolate from their measurements in the Monterey Canyon to estimate that the total rate of dissipation of energy from internal tides within the canyons on the continental slopes surrounding the ocean basins is about 12 GW.

or

$$Q/U_1h_1 \int_0^1 F_1(x)dx = P - 1, \tag{A5}$$

where an entrainment factor,

$$P = U_2h_2 \int_0^1 F_2(x)dx \Bigg/ \left(U_1h_1 \int_0^1 F_1(x)dx \right), > 1, \tag{A6}$$

is a measure of the entrainment.

The conservation of mass flux leads, in general, with Eq. (A3) to a further relation:

$$U_1h_1 \int_0^1 f_1(x)F_1(x)dx = U_2h_2 \int_0^1 f_2(x)F_2(x)dx, \tag{A7}$$

so that Eq. (A6) can be written

$$P = \int_0^1 f_1(x)F_1(x)dx \int_0^1 F_2(x)dx \Bigg/ \left(\int_0^1 f_2(x)F_2(x)dx \int_0^1 F_1(x)dx \right). \tag{A8}$$

Momentum conservation (conservation of $\int pdz + \int(\rho U)Udz$, where p is the pressure, assumed to be hydrostatic upstream and downstream of a transition) leads, after a little algebra, to

$$\begin{aligned} U_2^2h_2 \int_0^1 F_2^2(x)dx - U_1^2h_1 \int_0^1 F_1^2(x)dx \\ = 2g\beta \left[h_1^2 \int_0^1 \int_x^1 f_1(y)dydx - h_2^2 \int_0^1 \int_x^1 f_2(y)dydx \right], \end{aligned} \tag{A9}$$

where g is the acceleration due to gravity. Writing $q = h_2/h_1$ and, using Eq. (A7),

$$U_2 = U_1 \int_0^1 f_1(x)F_1(x)dx \Bigg/ \left(q \int_0^1 f_2(x)F_2(x)dx \right), \tag{A10}$$

Eq. (A9) gives

$$U_1^2/g\beta h_1 = 2q\left[q^2\int_0^1\int_x^1 f_2(y)dydx - \int_0^1\int_x^1 f_1(y)dydx\right]\Bigg/$$

$$\left[\int_0^1 F_1^2(x)dx\left\{q - P^2\int_0^1 F_2^2(x)dx\left(\int_0^1 F_1(x)dx\right)^2\right\}\Bigg/\right. \tag{A11}$$

$$\left.\left[\int_0^1 F_1^2(x)dx\left(\int_0^1 F_2(x)dx\right)^2\right]\right],$$

as a condition for a transition to occur.

In general, the nondimensional loss in energy flux per unit channel width, ΔE (the change in the sum of the kinetic energy flux, $\int(\rho U^2/2)Udz$, and the potential energy flux, $\int g\rho zUdz$, accounting for the work done by the pressure force, $\int pUdz$) can be written as

$$\begin{aligned}
&\Delta E/(g\rho\beta U_1 h_1^2)\\
&= (U_1^2/2g\beta h_1)\left\{\int_0^1 F_1^3(x)dx - \int_0^1 F_2^3(x)dx\left[\int_0^1 f_1(x)F_1(x)dx\Big/\int_0^1 f_2(x)F_2(x)dx\right]^3\Big/q^2\right\}\\
&\quad + 2\left[\int_0^1 xF_1(x)dx - \int_0^1 xf_1(x)F_1(x)dx + \int_0^1 F_1(x)\int_x^1 f_1(y)dydx\right]\\
&\quad - 2q\left[\int_0^1 f_1(x)F_1(x)dx\Big/\int_0^1 f_2(x)F_2(x)dx\right]\\
&\quad \times\left[\int_0^1 xF_2(x)dx - \int_0^1 xf_2(x)F_2(x)dx + \int_0^1 F_2(x)\int_x^1 f_2(y)dydx\right],
\end{aligned} \tag{A12}$$

provided that the kinetic energy flux carried by the entrained flow is negligible, with $U_1^2/g\beta h_1$ given by Eq. (A11). With no source of energy in the transition, ΔE must not be negative.

As in model A, the flow downstream of a transition may be regarded as unstable if a further transition is possible with no entrainment. Proceeding as in Section 3, we find that the condition for instability is

$$\begin{aligned}
U_1^2/g\beta h_1 > 4q^3&\left[\int_0^1\int_x^1 f_2(y)dydx\Big/\int_0^1 F_2^2(x)dx\right]\\
&\times\left[\int_0^1 f_2(x)F_2(x)dx\Big/\int_0^1 f_1(x)F_1(x)dx\right]^2 f_2(0).
\end{aligned} \tag{A13}$$

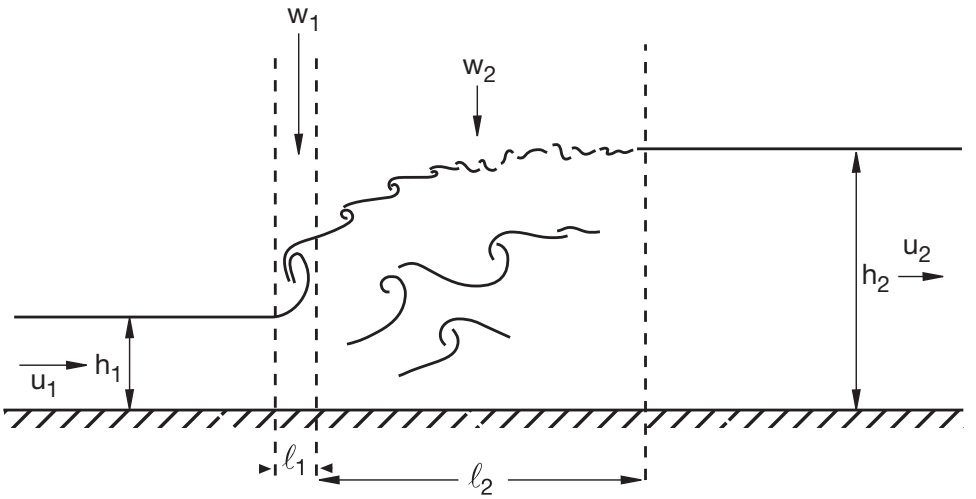

Figure A1. Sketch of the entrainment in a hydraulic jump.

APPENDIX B

The kinetic energy flux of the entrained fluid

Observations of internal transitions, such as those of the image of a hydraulic jump in the lee of the Sierra Nevada shown by Turner (1973; his Figure 3.11) or the relatively weak transitions described by Wilkinson and Wood (1971), suggest that entrainment into the moving water may occur rapidly at the leading edge or toe of the transition, where an overturning, rotor-like structure or clefts and lobes akin to those in a gravity current (Simpson, 1997) may form, and more slowly within a more conventional entraining flow leading eventually to a relatively steady flow downstream. As sketched in Figure A1, we suppose that entrainment at the toe occurs at a rate, w_1, is proportional to the speed of the moving layer, U_1 or u_{max}, and over a length, l_1, proportional to h_1 or the height of the velocity maximum, $0.182h_1$, in models A and B respectively. In the following region, the entrainment rate, w_2, is proportional to the maximum flow speed downstream of the transition over a length, l_2, proportional to h_2. The total entrainment flux is

$$Q = w_1 l_1 + w_2 l_2, \tag{A13}$$

where $w_1 = e_1 U_1$, $w_2 = e_2 U_2$, $l_1 = \lambda_1 h_1$ and $l_2 = \lambda_2 h_2$, and where e_1, e_2, λ_1 and λ_2 are constants of proportionality. The ratio of the flux of entrained kinetic energy, KE_E, to the flux of kinetic energy in the flow ahead of the transition, KE_1, [either $\rho U_1^3 h_1 (1 - r_1/2)/2$ for model A or $\rho U_1^3 \int F_1^3 dx/2$ for model B] is

$$\Lambda = \rho(w_1^3 l_1 + w_2^3 l_2)/2KE_1, \tag{A14}$$

and this can be evaluated with suitable choices of the constants of proportionality which must be chosen to be consistent with Eq. (A13).

For model A, using Eqs. (5) and (6), Eq. (A13) can be expressed in terms of the entrainment ratio, Q/U_1h_1:

$$e_1\lambda_1 + 1 = (1 + Q/U_1h_1)(1 - e_2\lambda_2), \tag{A15}$$

whilst Eq. (A14) leads to

$$\Lambda = [2/(2 - r_2)][e_1^3\lambda_1 + e_2^3\lambda_2(1 + Q/U_1h_1)^3/q^2]. \tag{A16}$$

For probable values of e_2 (< 0.1; see Turner, 1974) and $\lambda_2 = O(5)$, Λ is dominated by the entrainment at the toe. Maximising this term by taking $e_2 = 0$, and selecting $\lambda_1 = 1$, Eq. (A15) gives $e_1 = Q/U_1h_1$ and Eq. (A16) gives $\Lambda = [2/(2 - r_2)](Q/U_1h_1)^3$. For the range of r_1 and r_2 of Table 1, we find that $2.16 \times 10^{-6} < \Lambda < 0.0526$. The ratio, $KE_E/\Delta E$, of the flux of entrained kinetic energy to the estimated rate of loss of energy flux disregarding the entrained kinetic energy flux, lies between 3.13×10^{-5} and 0.246, with all values except that at $r_1 = 0.8$, $r_2 = 0.8$, $q = 2.4$, being less than 0.08. We conclude that the values of ΔE in Table 1, whilst underestimating the rate of loss of energy flux, are unlikely to do so by more than 30%.

For model B, taking $P = 1.316 = Q/\ U_1h_1\int F_1 dx + 1$, and substituting values for the velocity profile function, F_1, from Eq. (15) into Eq. (A13) we find

$$e_1\lambda_1/2 + 2.087e_2\lambda_2 = 0.316, \tag{A17}$$

whilst Eq. (A14) gives

$$\Lambda = 0.82e_1^3\lambda_1 + 10.26e_2^3\lambda_2/q^2. \tag{A18}$$

Making the *ad hoc* choices, $e_1 = 0.3$, $e_2 = 0.05$, $\lambda_1 = 1$ and $\lambda_2 = 1.6$, values that are quite severely constrained to satisfy Eq. (A17), we find that the kinetic energy entrained at the toe dominates that in the following region, and that values of Λ are about 0.022. Comparing these with the values of $R = \Delta E/KE_1$ in Table 2, the entrained kinetic energy flux may be comparable to the loss in energy flux, ΔE, estimated disregarding the entrained kinetic energy flux, only for the smaller values of q when the estimated loss in energy flux is also small. When the loss in energy flux is more substantial, i.e., when $q > 5.5$ in Table 2, the neglected contribution of the entrained water is less than about 20%.

Acknowledgments. I am most grateful to Dr. Harry Bryden for discussions on the topic of mixing in channels connecting deep ocean basins. Dr. Alan Elliott allowed me to use a computer and Mrs. Kate Davis kindly helped in producing the figures. Mr. Baris Ozen generously provided profiles of velocity and density obtained from measurements made in $O(20$ m) thick layers of water cascading down the side of Lake Geneva during severe winter cooling conditions.

REFERENCES

Baines, P. G. 1995. Topographic Effects in Stratified Flows, Cambridge University Press, Cambridge, 482 pp.

Bryden, H. L. and A. J. Nurser. 2003. Effects of strait mixing on ocean stratification. J. Phys. Oceanogr., *33*, 1870–1872.

Ellison, T. H. and J. S.Turner. 1959. Turbulent entrainment in stratified fluids. J. Fluid Mech., *6*, 423–448.

Fer, I., U. Lemmin and S. A. Thorpe. 2002. Winter cascading of cold water in Lake Geneva. J. Geophys. Res., *107*, C6, 10.1029/2001JC000828, 13-1 to 16.

Ferron, B., H. Mercier, K. Speer, A. Gargett and K. Polzin. 1998. Mixing in the Romanche Fracture Zone. J. Phys. Oceanogr., *28*, 1929–1945.

Gregg, M. C., G. S. Carter and E. Kunze. 2005. Corrigendum. J. Phys. Oceanogr., *35*, 1712–1715.

Holland, D. M., R. R. Rosales, D. Stefanica and E. G. Tabak. 2002. Internal hydraulic jumps and mixing in two-layer flows. J. Fluid Mech., *470*, 63–83.

Mercier, H. and P. Morin. 1997. Hydrography of the Romanche and Chain Fracture Zones. J. Geophys. Res., *102*, 10,373–10,389.

Mercier, H. and K. G. Speer. 1998. Transport of bottom water in the Romanche Fracture Zone and the Chain Fracture Zone. J. Phys. Oceanogr., *28*, 779–790.

Munk, W. 1966. Abyssal recipes. Deep-Sea Res., *13*, 207–230.

Munk, W. and C. Wunsch. 1998. Abyssal recipes II, energetics of tidal and wind motion. Deep-Sea Res.I, *45*, 1977–2010.

Polzin, K., K. G. Speer, J. M. Toole and R. W. Schmitt. 1996. Intense mixing of Antarctic Bottom Water in the equatorial Atlantic Ocean. Nature, *380*, 54–56.

Simpson, J. E. 1997. Gravity Currents, 2nd ed., Cambridge University Press, Cambridge, 244 pp.

Thurnherr, A. M., L. C. St. Laurent, K. G. Speer, J. M. Toole and J. R. Ledwell. 2005. Mixing associated with sills in a canyon on the mid-ocean ridge flank. J. Phys. Oceanogr., *35*, 1370–1381.

Turner, J. S. 1973. Buoyant Effects in Fluids, Cambridge University Press, Cambridge, 367 pp.

Wesson, J. C. and M. C. Gregg. 1994. Mixing at the Camarinal Sill in the Strait of Gibraltar. J. Geophys. Res., *99*, 9847–9878.

Wilkinson, D. R. and I. R. Wood. 1971. A rapidly varied flow phenomenon in a two-layer flow. J. Fluid Mech., *47*, 241–256

Wunsch, C. and R. Ferrari. 2004. Vertical mixing, energy, and the general circulation of the ocean. Annu. Rev. Fluid Mech., *36*, 281–314.

Received: *4 November, 2005*; revised: *1 December, 2006.*